Structures 24 (2020) 73–86

Contents lists available at ScienceDirect

Structures

journal homepage: www.elsevier.com/locate/structures

# Simple equations for predicting the rotational ductility of fiber-reinforced-polymer strengthened reinforced concrete joints

Yazan B. Abu Tahnat[a], Mohammad A. Samaaneh[b,*], Mahmud M.S. Dwaikat[b], Abdulsamee M. Halahla[c]

[a] Department of Civil Engineering, Middle East Technical University, Ankara, Turkey
[b] Department of Civil Engineering, An-Najah National University, Nablus, Palestine
[c] Department of Civil Engineering, Fahad Bin Sultan University, Tabuk, Saudi Arabia

ARTICLE INFO

*Keywords:*
Fiber-Reinforced Polymer (FRP)
Ductility
Reinforced concrete joints
Finite Element modeling
ABAQUS
Nonlinear behavior
Simplified equations

ABSTRACT

Achieving a certain limit of rotational ductility in retrofitted reinforced concrete (R.C) joints is very important in the design of earthquake-resistant structures. Strengthening of R.C joints using wraps of fiber-reinforced polymers (FRP) is a common attractive technique and has an effect on the ductility of such joints. This study focuses on developing simple conceptual equations to predict the ductility of exterior reinforced concrete (R.C) beam-column joints as a function of the applied FRP. The equations are derived based on statistical regression through parametric study using results from a high-fidelity finite element model created using ABAQUS. The validated model includes material and geometric nonlinearities, in addition to the use of realistic nonlinear contact behavior between FRP and concrete. The proposed simple equations can be used as an initial conceptual design step for checking the adequacy of R.C beam-column joints in seismic design of R.C buildings. The proposed equations consider FRP, relative column-to-beam inertia, and transverse reinforcement in the beam and joint as the main parameter. This study defines the types of failure based on the ductility, and it develops the equations for ductile and brittle failures for both CFRP-strengthened joints and non-strengthened joints. This research confirms quantitatively the effectiveness of using CFRP to increase the ductility in most cases of the R.C beam-column joints. However, contribution of the CFRP is limited for some cases.

## 1. Introduction

Design of R.C beam-column joint has become a subject of interest for many researchers due to its unique importance in structures. RC beam–column joints are critical points in the structures because they are generally subjected to combined effect of many types of loadings. The combined effect of many types of loadings makes the behavior of such joints very complex and difficult to predict, especially under dynamic and reversal loadings [1,2].

The ACI-ASCE 352 (1985) [3] classifies the joints into two categories based on the type of the design loads and deformations:

1. Category 1: joints which are designed for strength only, without considering the ductility. This type is designed for gravity and normal wind loads.
2. Category 2: joints which are designed for sustained strength under deformation reversals into the inelastic range, thus requiring a certain limit of ductility. This type is designed to resist lateral loads such as earthquakes, blast and cyclonic winds.

Ductility describes the capacity of a material/section/member/structure to undergo large deformations without any significant reduction in strength. Material ductility, as determined from typical stress-strain curves, has the basic level of ductility which indicates the maximum ductility if all points of the structure have the same behavior and stressed equally which is difficult to happen. Sectional ductility is less than the material ductility because layers of materials in the section are not equally stressed under combined loading. Member ductility is further less than sectional ductility because the member generally yields at certain locations only. Finally, the structural ductility is the lowest because any structure consists of many members, in which plastic capacity is not reached at the same time.

Generally, ductility of a structure is affected mostly by joint failures [4]. Thus, ensuring sufficient rotational ductility at the joints can increase the overall structural ductility.

In the last decades, the use of Fiber Reinforced Polymer (FRP)

* Corresponding author.
*E-mail address:* m.samaaneh@najah.edu (M.A. Samaaneh).

https://doi.org/10.1016/j.istruc.2020.01.010
Received 3 September 2019; Received in revised form 10 November 2019; Accepted 6 January 2020
Available online 05 March 2020

**Table 1**
Description of the syllables used in naming the simulations.

| First syllable | | Second syllable | | Third syllable | | Fourth syllable | |
|---|---|---|---|---|---|---|---|
| Syllable | Meaning | Syllable | Meaning | Syllable | Meaning | Syllable | Meaning |
| G1 | 0.512 | MiJ | 0.5 $mm^2/mm$ | MiB | 0.5 $mm^2/mm$ | 0 | Without CFRP |
| G2 | 1 | MaJ | 4.5 $mm^2/mm$ | B1B | 1.13 $mm^2/mm$ | 1 | With CFRP |
| G3 | 4.63 | | | B2B | 3.14 $mm^2/mm$ | | |
| | | | | MaB | 4.5 $mm^2/mm$ | | |

composites presented an effective technique for strengthening concrete structures. Attari et al. [5] used CFRP, GFRP and hybrid FRP sheets to improve the flexural capacity of reinforced concrete beams. Moreover, this technique was used by many researchers and obtained good results such as Ghobarah and Said [6], El-Amoury [7], Mahmoud et al. [8], Samaaneh et al. [9] and Halahla et al. [10]. Moreover, Eslami and Ronagh [11] suggested a practical scheme of using CFRP sheets at the joints in a manner that takes cross beam and slab into consideration. They noticed that there was a remarkable enhancement in the load-carrying capacity and elastic stiffness of the CFRP-retrofitted joints. Esmaeeli et al. [12] implemented an effective technique to improve the seismic behavior of a damaged interior R.C beam-column joint by using a combination of strain hardening cementitious composite (SHCC) and laminates of carbon fibre reinforced polymers (CFRP laminates). Moreover, some researchers used externally bonded reinforcement on grooves (EBROG) method beside using CFRP sheets at the joint region so that the failure mode can be transferred to the beam rather than occurring at the joint. Moreover, by using this technique the debonding between CFRP and concrete surface was eliminated [13–17]. Fiber-section modeling approach was proposed by Mostofinejad et al. [18] to investigate the seismic behavior of RC beam column connections before and after the application of FRP retrofits. The results showed that the proposed model can predict the strength and displacement of un-retrofitted and FRP-retrofitted RC beam-column connections. Many parameters affect the ductility of R.C beam-column joints. For example, Jing et al. [19] concluded that the shear reinforcement within the joint is important for the improvement of the ductility. This observation was also numerically validated by Abu Tahnat et al. [20]. Other important parameters were examined by Abu Tahnat et al. [20] that affect the ductility of exterior R.C joints such as the relative column-to-beam gross inertia and the amount of transverse steel in the beam. The effect of lateral beams on the R.C joints was investigated by Hajrasouliha and Mostofinejad [21]. They found that the contribution of the lateral beam to the confinement of the joint is remarkable. Other parameters such as high strength concrete and steel rebars were studied by Alavi-Dehkordi et al. [22]. On the other hand, some parameters were observed to cause a slight positive effect on the capacity of the joint such as the axial force on column [23]

## 2. Parameters ranges and properties of the model

In this study, the experimentally-validated model created earlier by the authors [20] is used to generate the results of rotational ductility of R.C joints under various parameters. The numerical results are also validated through approximate simplified hand-calculation solutions, and then used to develop guidelines equations that predict ductility of R.C joints with and without FRP wraps.

The used range of parameters and a brief preview of the model are presented in this section. Further details of the model can be found in Abu Tahnat et al. [20].

### 2.1. Parameters ranges

Based on the sensitivity and parametric study conducted in an earlier study [20], four main parameters that were found to have an extreme effect on the ductility of R.C. joints are selected for the development of the equations. These parameters are relative gross inertia of column ($I_{gc}$) to beam ($I_{gb}$)($G = I_{gc}/I_{gb}$), shear reinforcement in joint$(Av/s)_J$, shear reinforcement in beam $(Av/s)_B$ and the effect of CFRP. A total of 48 nonlinear simulations have been conducted for R.C joints with and without CFRP. Each simulation is given a representative name comprising of 4 syllables, such as “G1-MaJ-MiB-0”. Generally, the first syllable in the name denotes the gross relative column-to-beam inertia, while the second syllable denotes the amount of stirrups inside the joint. The third syllable denotes the amount of stirrups in the beam; the final syllable denotes the use of CFRP. The numerical equivalence of each syllable is shown in Table 1.

All simulations with their parameters varied according to Table 2. On the other hand, the constant dimensions of the beam-column joint, which were considered for all models, are summarized in Table 3.

### 2.2. Finite element model

#### 2.2.1. Loading steps and boundary conditions

The generic overall model with its boundaries is shown in Fig. 1. It can be seen in this figure that the top end of the column is restrained by a rigid surface allowing the end to behave as a pin, while the bottom end is restrained by a rigid surface allowing the end to behave as a roller in the Y-direction to match the real behavior especially under the effect of lateral loads. It should be noted that these rigid surfaces restrain the in-plane movement of the column ends. Such restraint conditions are generally assumed for similar cases in the literature [24]. A constant axial load (0.26 $A_g f'_c$, where. *Ag*: is the gross sectional area of the column and $f'_c$ is the compressive strength of concrete) is initially applied to the column. This is followed by an incremental monotonic load (displacement control) applied to the tip of the beam as shown in Fig. 1. In order to validate the accuracy and reliability of the numerical model, the numerical load-deflection curve due to monotonic loading was compared with the envelopes of the loading hysteresis loops from the experimental test. It should be noted that this method of comparison between numerical and experimental results was adopted by many researchers [25,26].

The layout of the CFRP is assumed as wraps around the beam member with only one layer of CFRP sheet [20] as shown in Fig. 2. This schematic arrangement is selected as one of the effective strengthening techniques as stated by many researchers [27–29]. However, this arrangement of CFRP provides additional shear strength to the beam.

#### 2.2.2. Material models

*2.2.2.1. Concrete.* Concrete damage plasticity (CDP) model is used to define the complex nonlinear behavior of concrete. Moreover, this model takes confinements into consideration by using Biaxial and Triaxial stresses. In addition, the CDP model captures the degradation of the elastic stiffness in the strain softening branch of the stress-strain curve under compression ($d_c$) and tension ($d_t$). Wahalathantri et al. [30] defined the dc parameter as the ratio between the inelastic strain (crushing strain) and the total compression strain ($d_c = \varepsilon_{in}/\varepsilon_{cu}$), while the $d_t$ parameter is the ratio between the cracking strain and the total tension strain ($d_t = \varepsilon_{cr}/\varepsilon_t$). This model is based on the parameters summarized in Table 4. Default values of those parameters are

**Table 2**
The representative names and geometrical properties of all models.

| Model | Depth of beam ($h_b$) | $G$ | $(Av/s)_J$ | $(Av/s)_B$ | CFRP (Yes /No) |
|---|---|---|---|---|---|
| G1-MaJ-MiB-0 | 0.5 m | 0.512 | 4.5 | 0.5 | No |
| G1-MaJ-B1B-0 | 0.5 m | 0.512 | 4.5 | 1.13 | No |
| G1-MaJ-B2B-0 | 0.5 m | 0.512 | 4.5 | 3.14 | No |
| G1-MaJ-MaB-0 | 0.5 m | 0.512 | 4.5 | 4.5 | No |
| G2-MaJ-MiB-0 | 0.4 m | 1 | 4.5 | 0.5 | No |
| G2-MaJ-B1B-0 | 0.4 m | 1 | 4.5 | 1.13 | No |
| G2-MaJ-B2B-0 | 0.4 m | 1 | 4.5 | 3.14 | No |
| G2-MaJ-MaB-0 | 0.4 m | 1 | 4.5 | 4.5 | No |
| G3-MaJ-MiB-0 | 0.24 m | 4.63 | 4.5 | 0.5 | No |
| G3-MaJ-B1B-0 | 0.24 m | 4.63 | 4.5 | 1.13 | No |
| G3-MaJ-B2B-0 | 0.24 m | 4.63 | 4.5 | 3.14 | No |
| G3-MaJ-MaB-0 | 0.24 m | 4.63 | 4.5 | 4.5 | No |
| G1-MiJ-MiB-0 | 0.5 m | 0.512 | 0.5 | 0.5 | No |
| G1-MiJ-B1B-0 | 0.5 m | 0.512 | 0.5 | 1.13 | No |
| G1-MiJ-B2B-0 | 0.5 m | 0.512 | 0.5 | 3.14 | No |
| G1-MiJ-MaB-0 | 0.5 m | 0.512 | 0.5 | 4.5 | No |
| G2-MiJ-MiB-0 | 0.4 m | 1 | 0.5 | 0.5 | No |
| G2-MiJ-B1B-0 | 0.4 m | 1 | 0.5 | 1.13 | No |
| G2-MiJ-B2B-0 | 0.4 m | 1 | 0.5 | 3.14 | No |
| G2-MiJ-MaB-0 | 0.4 m | 1 | 0.5 | 4.5 | No |
| G3-MiJ-MiB-0 | 0.24 m | 4.63 | 0.5 | 0.5 | No |
| G3-MiJ-B1B-0 | 0.24 m | 4.63 | 0.5 | 1.13 | No |
| G3-MiJ-B2B-0 | 0.24 m | 4.63 | 0.5 | 3.14 | No |
| G3-MiJ-MaB-0 | 0.24 m | 4.63 | 0.5 | 4.5 | No |
| G1-MaJ-MiB-1 | 0.5 m | 0.512 | 4.5 | 0.5 | Yes |
| G1-MaJ-B1B-1 | 0.5 m | 0.512 | 4.5 | 1.13 | Yes |
| G1-MaJ-B2B-1 | 0.5 m | 0.512 | 4.5 | 3.14 | Yes |
| G1-MaJ-MaB-1 | 0.5 m | 0.512 | 4.5 | 4.5 | Yes |
| G2-MaJ-MiB-1 | 0.4 m | 1 | 4.5 | 0.5 | Yes |
| G2-MaJ-B1B-1 | 0.4 m | 1 | 4.5 | 1.13 | Yes |
| G2-MaJ-B2B-1 | 0.4 m | 1 | 4.5 | 3.14 | Yes |
| G2-MaJ-MaB-1 | 0.4 m | 1 | 4.5 | 4.5 | Yes |
| G3-MaJ-MiB-1 | 0.24 m | 4.63 | 4.5 | 0.5 | Yes |
| G3-MaJ-B1B-1 | 0.24 m | 4.63 | 4.5 | 1.13 | Yes |
| G3-MaJ-B2B-1 | 0.24 m | 4.63 | 4.5 | 3.14 | Yes |
| G3-MaJ-MaB-1 | 0.24 m | 4.63 | 4.5 | 4.5 | Yes |
| G1-MiJ-MiB-1 | 0.5 m | 0.512 | 0.5 | 0.5 | Yes |
| G1-MiJ-B1B-1 | 0.5 m | 0.512 | 0.5 | 1.13 | Yes |
| G1-MiJ-B2B-1 | 0.5 m | 0.512 | 0.5 | 3.14 | Yes |
| G1-MiJ-MaB-1 | 0.5 m | 0.512 | 0.5 | 4.5 | Yes |
| G2-MiJ-MiB-1 | 0.4 m | 1 | 0.5 | 0.5 | Yes |
| G2-MiJ-B1B-1 | 0.4 m | 1 | 0.5 | 1.13 | Yes |
| G2-MiJ-B2B-1 | 0.4 m | 1 | 0.5 | 3.14 | Yes |
| G2-MiJ-MaB-1 | 0.4 m | 1 | 0.5 | 4.5 | Yes |
| G3-MiJ-MiB-1 | 0.24 m | 4.63 | 0.5 | 0.5 | Yes |
| G3-MiJ-B1B-1 | 0.24 m | 4.63 | 0.5 | 1.13 | Yes |
| G3-MiJ-B2B-1 | 0.24 m | 4.63 | 0.5 | 3.14 | Yes |
| G3-MiJ-MaB-1 | 0.24 m | 4.63 | 0.5 | 4.5 | Yes |

**Table 3**
Constant dimensions of all models.

| Dimension name | Value (m) |
|---|---|
| Total length of beam ($L_{bt}$) | 0.9 |
| Total length of column ($L_c$) | 2.3 |
| Width of beam ($b_b$) | 0.4 |
| Width of column ($b_c$) | 0.4 |
| Depth of column ($h_c$) | 0.4 |

indicated in ABAQUS User's Manual [31].

Saenz model [32] as validated by Asran et al. [33] and Halahla et al. [34] is used to define the full stress–strain behavior of concrete under uniaxial compressive stress. On the other hand, the stress-strain curve for concrete under tension is tested experimentally by Sharif et al. [35] for concrete of compressive strength 25 MPa. The maximum tensile stress was reported as 2.9 MPa corresponding to modulus of rupture of concrete which is equal to $0.62\sqrt{f`_c}$ according to ACI 318 [36], and maximum strain of 0.003. Acceptable results were achieved by Abu Tahnat et al. [20] considering the mentioned tensile and compressive concrete behavior.

The compressive strength of concrete used in these models is 25 MPa with modulus of elasticity equals 23500 MPa as used by Abu Tahnat el al. [20]. Fig. 3 shows the required concrete input data for the CDP model in ABAQUS. It can be seen that Fig. 3a shows the uniaxial compression stress-inelastic strain curve of concrete, while Fig. 3b shows the tension stress-cracking strain. Also, Fig. 3c shows the compression damage parameter versus the inelastic strain curve, while Fig. 3d shows the tension damage parameter versus the cracking strain curve.

*2.2.2.2. Steel.* Elastic-perfectly plastic model is used in this work for the definition of steel material with yield strength of 285 MPa for stirrups, while yield strength of the longitudinal reinforcement is taken equal to 420 MPa. However, all of the steel have Young's Modulus (E = 205GPa) and Poisson's Ratio ($\nu$ = 0.3) as reported by Sharif et al. [35].

*2.2.2.3. CFRp.* Unidirectional CFRP sheets are used to strengthen the R.C beam-column joint model. The fiber behavior is linear elastic up to the rupture failure. A lamina linear elastic element is used to model the CFRP as shown in Fig. 4. The properties of the CFRP and epoxy material that was used by Abu Tahnat et al. [20] are summarized in Tables 5 and 6, respectively.

The mechanical properties of the combined CFRP sheet and adhesive material are shown in Table 7 and these values are evaluated according to Mallick's proposed equations [37].

*2.2.3. Modeling of interfaces*

Different contact models are used to model the interfacial region depending on the actual behavior and the degree of accuracy. Tie contact is used between beam and column parts. The same type of contact is also used between loading plate and beam. This contact considers perfect bond between two surfaces to make the translational and rotational motion as well as the motions corresponding to all other active degrees of freedom equal for a pair of surfaces. The contact between reinforcement and concrete is assumed to be perfectly bonded surface with no slip. This is justified by the adequate development length of rebar and the available friction between them, therefor, embedded region contact is used to simulate the perfect bond. Cohesive contact is used to simulate the behavior of adhesive material between concrete and CFRP. Both separation-traction and force-slip constitutive curves are needed to model the cohesive behavior. Many models exist with various degrees of complexity. The linear-brittle model, developed by Neubauer and Rostasy [38] is used to model the cohesive contact as shown in Fig. 5 with initial shear stiffness ($K_0$) and shear strength ($t_{max}$) equal to those proposed by Obaidat et al [39] as shown in Eqs. (1) and (2). However, the maximum normal strength can be considered equal to the tensile strength of concrete [39]. On the other hand, normal stiffness ($K_{nn}$) is assumed equal to shear stiffness ($K_{ss}$ and $K_{tt}$) as there is no sufficient data available about it with the use of adequate development length and sheeting wraps. However, the same model was compared to the tie contact model and showed no differences. The verified experimental beam-column joints did not report any de-bonding of the FRP. Values are considered equal to 1300 (N/mm$^3$) [20].

$$K_0 = 0.16\frac{G_a}{t_a} + 0.47 \quad (1)$$

$$t_{max} = 1.46{G_a}^{0.165}{f_{ct}}^{1.033} \quad (2)$$

where:

$K_0$: Initial shear stiffness (GPa)
$G_a$: Shear modulus of adhesive (GPa)
$t_a$: Adhesive thickness (mm)
$f_{ct}$: Tensile strength of concrete (MPa)

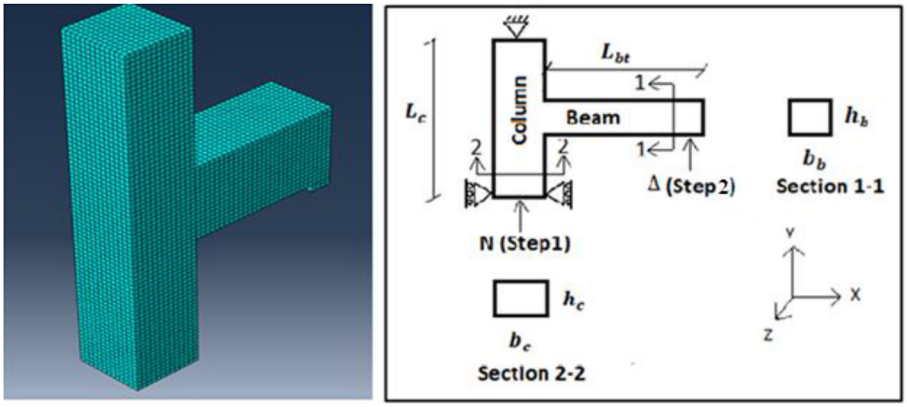


**Fig. 1.** F.E. Model and location of loads and boundary conditions [20].

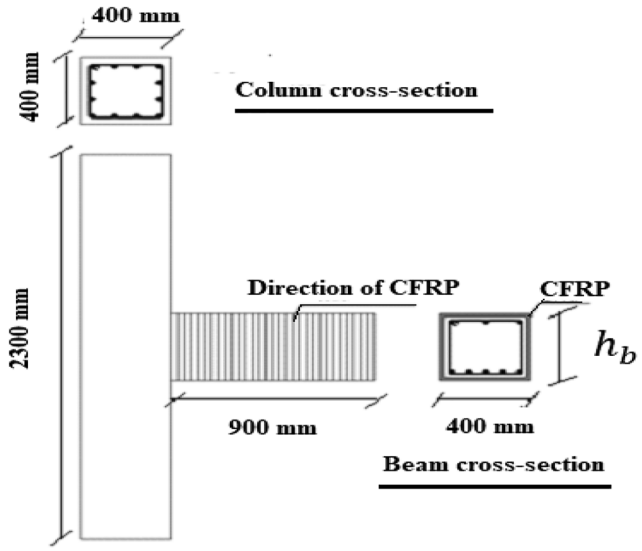


**Fig. 2.** Typical wrapping arrangement of CFRP [20].

**Table 4**
Parameters of CDP model.

| Parameter name | Value |
|---|---|
| Dilation angle (ψ) | 36° |
| Eccentricity (e) | 0.1 |
| $f_{b0}/f_{c0}$ | 1.16 |
| K | 0.667 |

$t_{max}$: Shear strength for cohesive interaction (MPa)

#### 2.2.4. Meshing type and sensitivity study

The components of the beam-column joint are meshed individually on a part-by-part basis instead of using global or sweep mesh. Eight-Nodded linear brick element (C3D8R) is used to model the solid elements; concrete and plate. A 2-node linear 3-D truss element is used to model main and transverse reinforcement (T3D2), whereas 4-noded shell element (S4R) is used to model the CFRP as shown in Fig. 6. Sensitivity study is conducted to eliminate the effect of mesh size on the accuracy of results. Different global mesh sizes are considered (15 mm through 45 mm). The results show that the resulting curves stabilize approximately for meshes of range sizes 15–35 mm as shown in Fig. 7. However a mesh size of 15 mm is used in all subsequent models to show the cracks accurately.

## 3. Generic behavior of R.C. joints

The general features of a typical load-deflection curve of the R.C beam-column joint is shown in Fig. 8. The behavior of the beam-column joint is initially linear elastic up to the development of beam cracks close to the beam-column interface (tension zoon). This could be noticed by a simple drop in the load-deflection curve. The tensile force is resisted later by the tension reinforcement where the beam continues elastically up to the yielding of the tension steel. Beyond this stage, the behavior is controlled by the reinforcement details and the strengthening techniques. Based on that, brittle shear failure or ductile flexural failure may happen.

### 3.1. Failure criteria

The rotational ductility is defined as the ultimate deflection divided by the yield deflection.

In order to calculate the rotational ductility of the joint from the resulting load-deflection curves, a criterion is needed to specify the yield and ultimate deflections. First, the yield deflection is taken to be the stage at which tensile steel starts to yield. The ultimate deflection is considered to be the instant when the load-deflection curve goes below 85% of the peak capacity [40]. This criterion is applied for all curves regardless of the type of failure.

### 3.2. Failure modes

Different types of failure modes may happen in the simulated exterior R.C beam-column joints. Failure mode is controlled by many parameters such as the amount of shear reinforcement inside the joint $(Av/s)_J$, the amount of shear reinforcement in the beam $(Av/s)_B$, the relative gross inertia between the beam and the column($G$), and the existence of CFRP as stated earlier. Generally, the types of failure can be divided into three categories. The first is ductile beam failure, another one is brittle beam failure, and an intermediate case called joint failure. These failure modes are illustrated in this section with clear examples. It should be noticed that the definition of ductile failure in this work is the failure which does not happen suddenly.

#### 3.2.1. Ductile beam failure

This type of failure is characterized by crushing of concrete at the compression zone of the beam after yielding of tension beam bars. This failure mode is called flexural failure in the beam (FB-D). For instance, the failure occurred in model (G3-MaJ-MaB-0), which represents a beam-column joint without CFRP including $(Av/s)_J$ = 4.5 mm$^2$/mm, $(Av/s)_B$ = 4.5 mm$^2$/mm and relative inertia($G$) = 4.63, is a good example of FB-D failure. The obtained F.E. response of this joint is shown in Fig. 9 and the mentioned general features (marked from 1 to 4) can

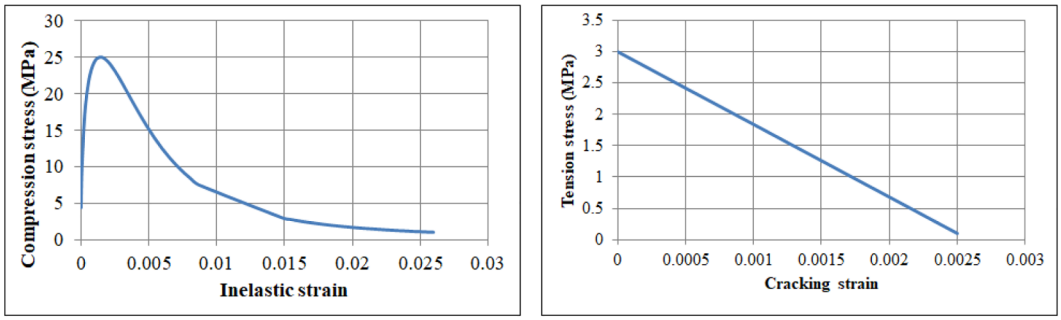


(a) Compressive stress vs. Inelastic strain

(b) Tensile stress vs. Cracking strain

(c) Compressive damage vs. Inelastic strain

(d) Tensile damage vs. Cracking strain

**Fig. 3.** Definition of concrete parameters for the CDP model for concrete 25 MPa.

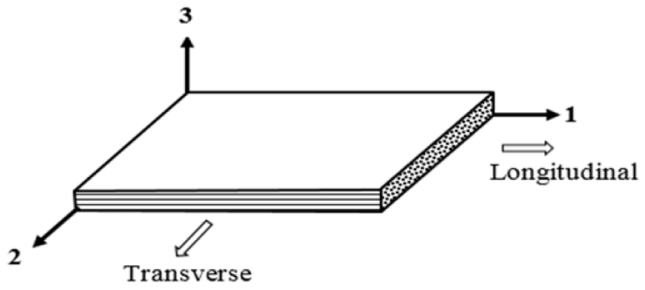


**Fig. 4.** Schematic of unidirectional FRP lamina.

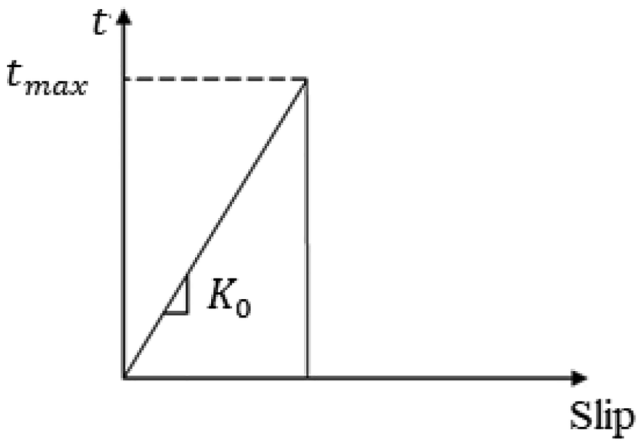


**Fig. 5.** Bond-slip curve model [38].

**Table 5**
Properties of CFRP sheets.

| Ultimate tensile strength (MPa) | Ultimate strain (%) | Modulus of elasticity (MPa) | Thickness (mm) |
|---|---|---|---|
| 3500 | 1.5 | 230,000 | 0.13 |

**Table 6**
Properties of epoxy.

| Tensile strength (MPa) | Tensile modulus (MPa) | Ultimate elongation (%) |
|---|---|---|
| 30 | 21,400 | 4.8 |

be clearly seen from the curve. Point (1) represents tensile cracking in the beam. A 3D view of the axial stress ($S_{33}$) in the beam at this stage is shown in Fig. 10. Point (2) represents yielding of the tension steel and Fig. 11 shows a 3D view of the longitudinal stress in steel at this limit. Point (3) represents the maximum principle compressive stress in concrete at the top layer of the compression zone in the beam. At this point, the compression stress starts to decrease. Point (4) represents the flexure failure of the joint due to crushing of the beam concrete. Beyond this point, the joint is no longer capable of resisting imposed rotations. Distribution of plastic strain clearly shows that the type of failure is

**Table 7**
Properties of combined FRP sheets with adhesive materials.

| Combined CFRP Thickness (mm) | $E_1$ (MPa) | $E_2$ (MP) | $\nu_{12}$ | $G_{12}$ (MPa) | $G_{13}$ (MPa) | $G_{23}$ (MPa) |
|---|---|---|---|---|---|---|
| 1.631 | 106,509 | 33,970 | 0.31 | 12,400 | 12,400 | 13,065 |

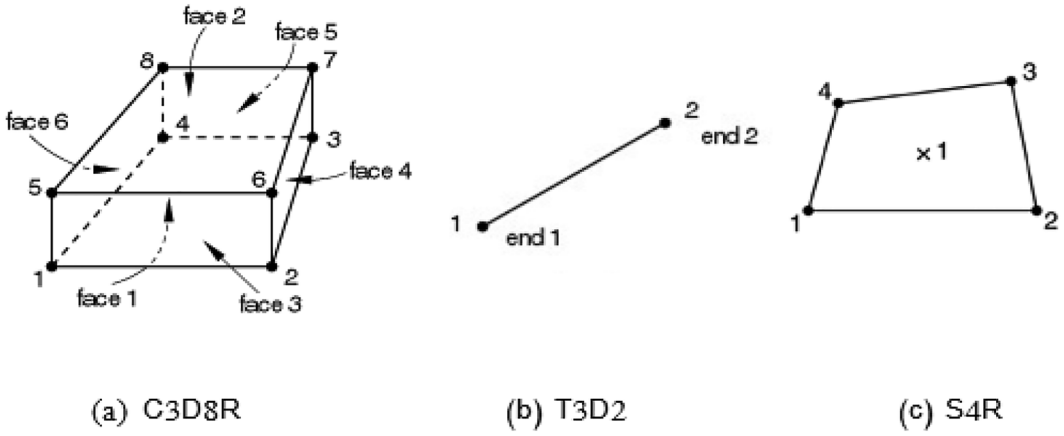


**Fig. 6.** F.E. Mesh Type.

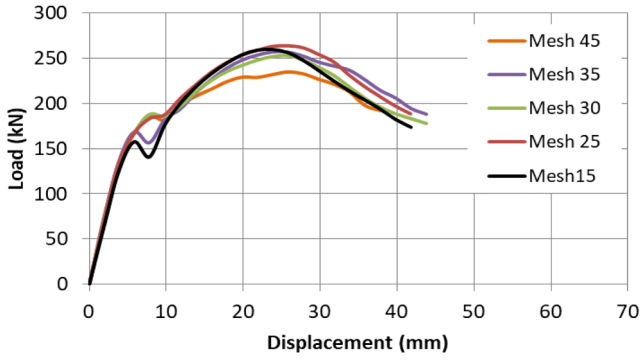


**Fig. 7.** Effect of mesh size.

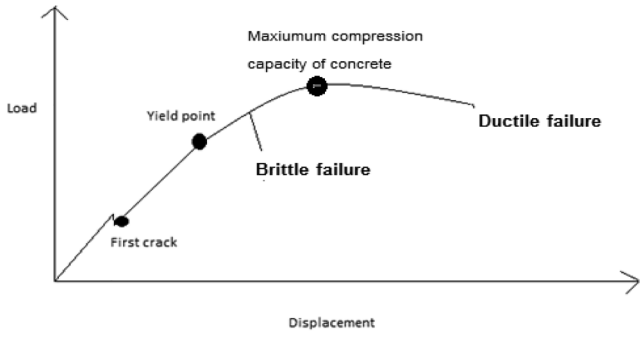


**Fig. 8.** Typical load–deflection curve for joints.

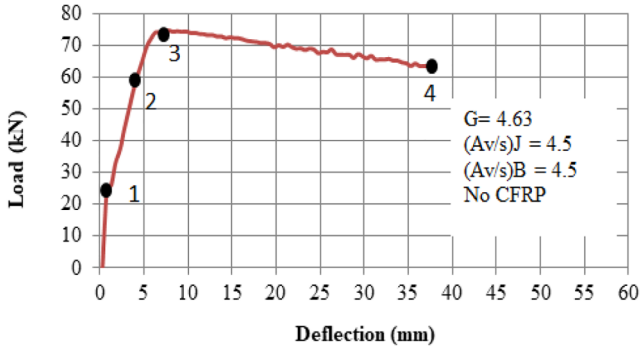


**Fig. 9.** Load–deflection curve for joint (G3-MaJ-MaB-0) with the stages of behavior.

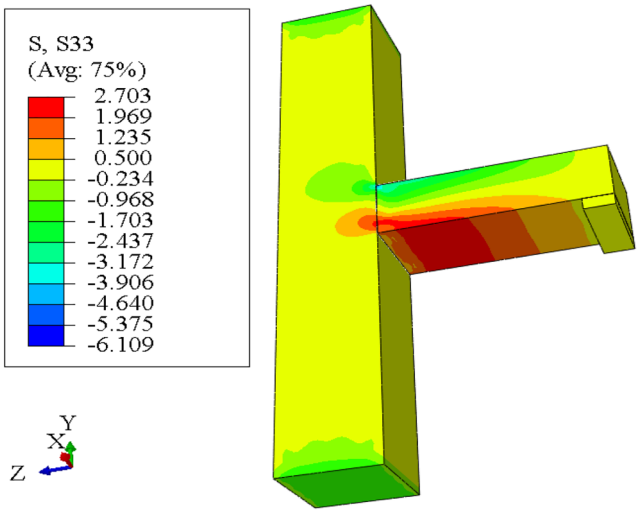


**Fig. 10.** Cracking of the beam for joint (G3-MaJ-MaB-0) (Normal stress in MPa).

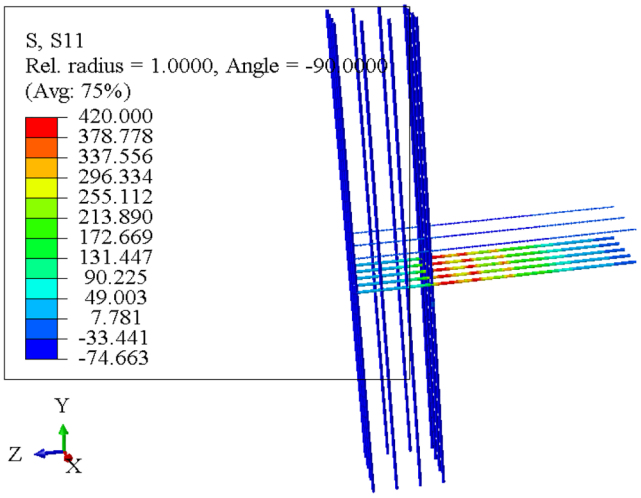


**Fig. 11.** Yielding of steel for joint (G3-MaJ-MaB-0) (Tensile stress in MPa).

flexural failure due to the damage of concrete at the compression zone of the beam as shown in Fig. 12. In addition, Fig. 13 shows the compression damage of concrete at this stage.

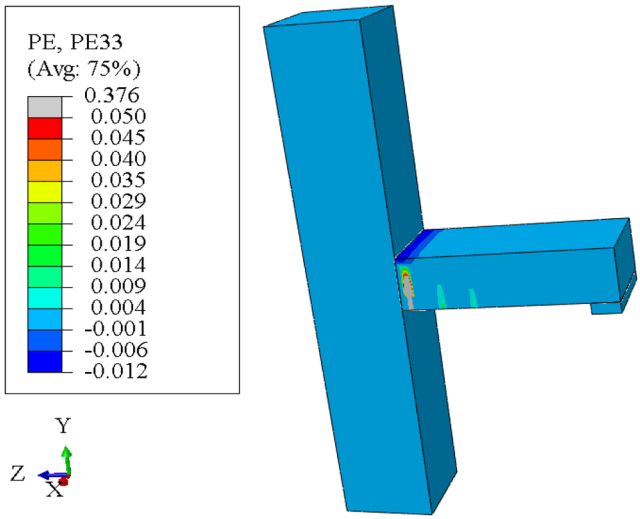


**Fig. 12.** Plastic Strain distribution at the beam for joint (G3-MaJ-MaB-0).

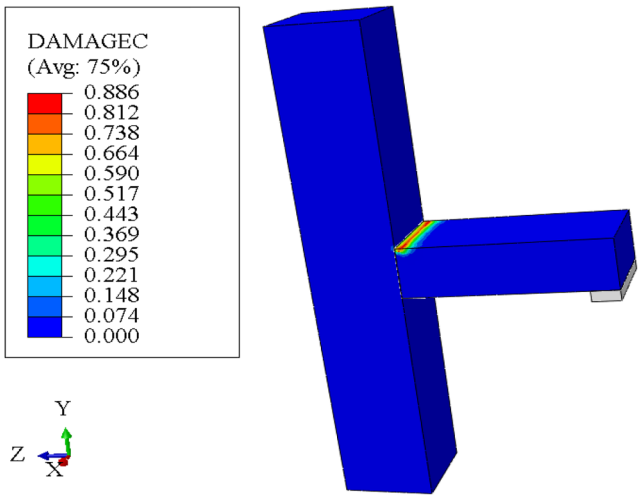


**Fig. 13.** Compression damage of concrete for joint (G3-MaJ-MaB-0).

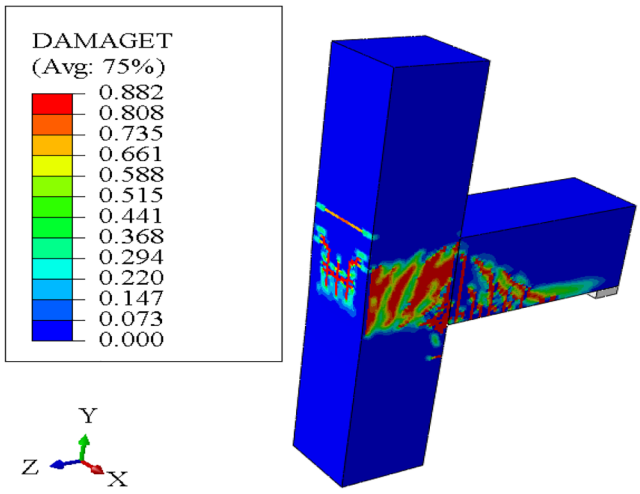


**Fig. 14.** Tension damage of the concrete beam for joint (G1-MiJ-MaB-0).

### 3.2.2. Joint failure

This type of failure happens due to insufficient strength of stirrups inside the joint to resist the combined shear and tensile forces (JF). It should be noted that the ductility of this type of failure is less than the ductility of flexural failure of the beam and more than the ductility of the shear failure of the beam. However, ductility of this type of failure is controlled by the axial load in the column as higher axial load reduces the resultant principal tensile stresses inside the joint. Failure occurred in model (G1-MiJ-MaB-0), which represents a beam-column joint without CFRP including $(Av/s)_J$ = 0.5 mm$^2$/mm, $(Av/s)_B$ = 4.5 mm$^2$/mm and relative inertia($G$) = 0.512, is a good example of joint failure. This type of failure. The obtained F.E. tension damage of this type of failure is shown in Fig. 14. It should be noted that ductility values of this type of failure are relatively closer to those related to the flexural failure mode in the beam, therefore, ductility of these joints can be predicted using the proposed ductility equation introduced later in this paper.

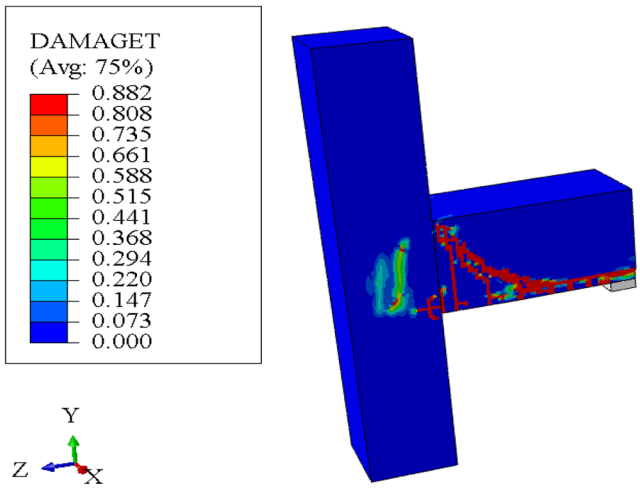


**Fig. 15.** Complete tension damage of the concrete beam for joint (G1-MaJ-MiB-0).

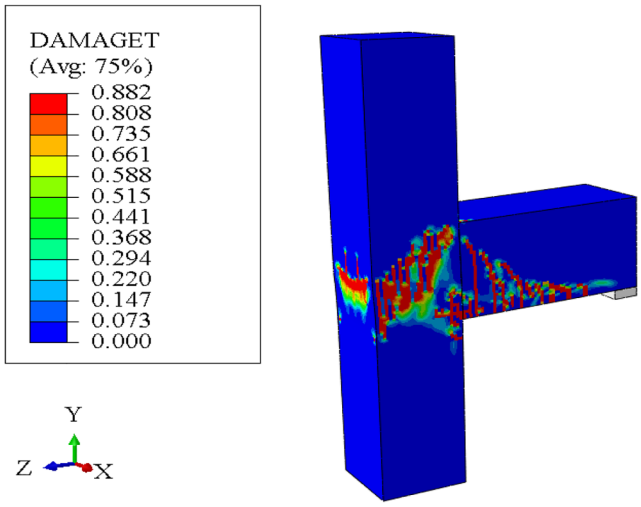


**Fig. 16.** Complete tension damage of the concrete beam for joint (G1-MiJ-MiB-R).

### 3.2.3. Brittle failure

Brittle failure includes one of the following:

1- Shear failure in the beam (SB-B). This type of failure happens due to insufficient strength of stirrups inside the beam to resist shear force, therefore, this type of failure could be avoided by using CFRP. However, the failure occurred in model (G1-MaJ-MiB-0), which represents a beam-column joint without CFRP including $(Av/s)_J$ = 4.5 mm$^2$/mm, $(Av/s)_B$ = 0.5 mm$^2$/mm and relative

**Table 8**
Summary of F.E. results.

| Model | $P_y$ (kN) | $P_P$ (kN) | $0.85P_p$ (kN) | $\Delta_y$ (mm) | $\Delta_p$ (mm) | $\Delta_u$ (mm) | Ductility ($\frac{\Delta_u}{\Delta_y}$) | Failure mode |
|---|---|---|---|---|---|---|---|---|
| G1-MaJ-MiB-0 | 350 | 360 | 306 | 6.28 | 7.8 | 7.8 | 1.24 | SB-B |
| G1-MaJ-B1B-0 | 360 | 400 | 340 | 6.28 | 8.7 | 10.27 | 1.64 | SB-B |
| G1-MaJ-B2B-0 | 366.4 | 416.2 | 353.77 | 6.28 | 10.2 | 20.27 | 3.23 | FB-D |
| G1-MaJ-MaB-0 | 366.5 | 417 | 354.45 | 6.28 | 10.2 | 20.3 | 3.23 | FB-D |
| G2-MaJ-MiB-0 | 210 | 260.2 | 221.17 | 5 | 7.4 | 8.8 | 1.76 | SB-B |
| G2-MaJ-B1B-0 | 220 | 274 | 232.9 | 5 | 7.4 | 22.26 | 4.45 | FB-D |
| G2-MaJ-B2B-0 | 230 | 274.5 | 233.325 | 5 | 7.4 | 23 | 4.6 | FB-D |
| G2-MaJ-MaB-0 | 230 | 275 | 233.75 | 5 | 7.4 | 23 | 4.6 | FB-D |
| G3-MaJ-MiB-0 | 69 | 74.5 | 63.325 | 5.2 | 7.5 | 37.8 | 7.27 | FB-D |
| G3-MaJ-B1B-0 | 69 | 74.8 | 63.58 | 5.2 | 7.5 | 38 | 7.31 | FB-D |
| G3-MaJ-B2B-0 | 69 | 75 | 63.75 | 5.2 | 7.5 | 38.3 | 7.37 | FB-D |
| G3-MaJ-MaB-0 | 69 | 75 | 63.75 | 5.2 | 7.5 | 38.5 | 7.4 | FB-D |
| G1-MiJ-MiB-0 | 310 | 330.1 | 280.585 | 6.5 | 10.2 | 13.1 | 1.95 | JSB-B |
| G1-MiJ-B1B-0 | 310 | 347 | 294.95 | 6.7 | 10.2 | 18.266 | 2.73 | JF |
| G1-MiJ-B2B-0 | 315 | 347 | 294.95 | 6.7 | 10.2 | 18.76 | 2.8 | JF |
| G1-MiJ-MaB-0 | 315 | 347 | 294.95 | 6.7 | 10.2 | 18.77 | 2.8 | JF |
| G2-MiJ-MiB-0 | 220 | 249 | 211.65 | 5 | 9 | 14.5 | 2.9 | JSB-B |
| G2-MiJ-B1B-0 | 225 | 249 | 211.65 | 5 | 9 | 19.76 | 4 | JF |
| G2-MiJ-B2B-0 | 225 | 249 | 211.65 | 5 | 9 | 19.8 | 4 | JF |
| G2-MiJ-MaB-0 | 225 | 250.6 | 213.01 | 5 | 9 | 19.81 | 4 | JF |
| G3-MiJ-MiB-0 | 69 | 74.5 | 63.325 | 5.2 | 7.5 | 37.78 | 7.27 | FB-D |
| G3-MiJ-B1B-0 | 69 | 74.5 | 63.325 | 5.2 | 7.5 | 37.78 | 7.27 | FB-D |
| G3-MiJ-B2B-0 | 69 | 74.5 | 63.325 | 5.2 | 7.5 | 38 | 7.31 | FB-D |
| G3-MiJ-MaB-0 | 69 | 74.5 | 63.325 | 5.2 | 7.5 | 38 | 7.31 | FB-D |
| G1-MaJ-MiB-1 | 370 | 408 | 346.8 | 6.28 | 7.8 | 19 | 3.03 | FB-D |
| G1-MaJ-B1B-1 | 370 | 408.5 | 347.225 | 6.28 | 8.7 | 19 | 3.03 | FB-D |
| G1-MaJ-B2B-1 | 370 | 417.6 | 354.96 | 6.28 | 10.2 | 19.5 | 3.1 | FB-D |
| G1-MaJ-MaB-1 | 370 | 418 | 355.3 | 6.28 | 10.2 | 19.5 | 3.1 | FB-D |
| G2-MaJ-MiB-1 | 230 | 277 | 235.45 | 5 | 7.4 | 22.25 | 4.45 | FB-D |
| G2-MaJ-B1B-1 | 230 | 277 | 235.62 | 5 | 7.4 | 22.25 | 4.45 | FB-D |
| G2-MaJ-B2B-1 | 230 | 279 | 237.15 | 5 | 7.4 | 23.25 | 4.65 | FB-D |
| G2-MaJ-MaB-1 | 230 | 280 | 238 | 5 | 7.4 | 23.25 | 4.65 | FB-D |
| G3-MaJ-MiB-1 | 70 | 75 | 63.75 | 5.2 | 7.5 | 38 | 7.31 | FB-D |
| G3-MaJ-B1B-1 | 70 | 75 | 63.75 | 5.2 | 7.5 | 38 | 7.31 | FB-D |
| G3-MaJ-B2B-1 | 70 | 75 | 63.75 | 5.2 | 7.5 | 38.4 | 7.38 | FB-D |
| G3-MaJ-MaB-1 | 70 | 75 | 63.75 | 5.2 | 7.5 | 38.7 | 7.44 | FB-D |
| G1-MiJ-MiB-1 | 302 | 347 | 294.95 | 6.7 | 10.2 | 18.25 | 2.72 | JF |
| G1-MiJ-B1B-1 | 302 | 347 | 294.95 | 6.7 | 10.2 | 18.25 | 2.72 | JF |
| G1-MiJ-B2B-1 | 302 | 347 | 294.95 | 6.7 | 10.2 | 18.7 | 2.79 | JF |
| G1-MiJ-MaB-1 | 302 | 347 | 294.95 | 6.7 | 10.2 | 18.7 | 2.79 | JF |
| G2-MiJ-MiB-1 | 216 | 246 | 209.1 | 5 | 9 | 19.7 | 3.94 | JF |
| G2-MiJ-B1B-1 | 216 | 247 | 209.95 | 5 | 9 | 20 | 4 | JF |
| G2-MiJ-B2B-1 | 216 | 248 | 210.8 | 5 | 9 | 20.2 | 4.04 | JF |
| G2-MiJ-MaB-1 | 216 | 250 | 212.5 | 5 | 9 | 20.4 | 4.08 | JF |
| G3-MiJ-MiB-1 | 70 | 75 | 63.75 | 5.2 | 7.5 | 38 | 7.31 | FB-D |
| G3-MiJ-B1B-1 | 70 | 75 | 63.75 | 5.2 | 7.5 | 38 | 7.331 | FB-D |
| G3-MiJ-B2B-1 | 70 | 75 | 63.75 | 5.2 | 7.5 | 38.4 | 7.38 | FB-D |
| G3-MiJ-MaB-1 | 70 | 75 | 63.75 | 5.2 | 7.5 | 38.7 | 7.44 | FB-D |

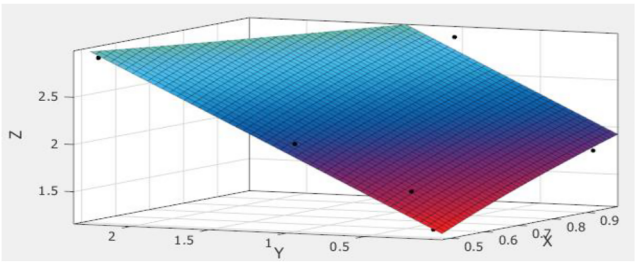


**Fig. 17.** Surface ductility fitting for joints without CFRP with brittle failure.

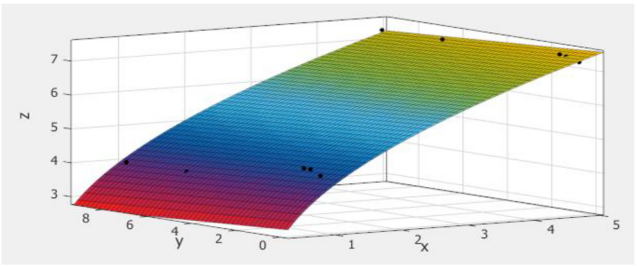


**Fig. 18.** Surface ductility fitting for joints without CFRP with ductile failure.

inertia($G$) = 0.512, is a good example of the shear failure in the beam. The obtained F.E. tension damage of concrete is shown in Fig. 15.

2- Simultaneous joint failure and shear failure in the beam (JSB-B). The sequence of failure is similar to (SB-B) but with shear failure happening in the beam and the joint at the same time. A good example of this failure is the one occurred in model (G1-MiJ-MiB-R), which represents a beam-column joint without CFRP including $(Av/s)_J$ = 0.5 mm$^2$/mm, $(Av/s)_B$ = 0.5 mm$^2$/mm and relative inertia($G$) = 0.512. The obtained F.E. tension damage of this type of failure is shown in Fig. 16.

Table 8 summarizes the main features of all simulations which are developed from the F.E and failure modes. These main features include; yield force ($P_y$), Peak force ($P_p$), force which goes under 85% of the peak

**Table 9**
Properties of random joints without CFRP.

| Model | $h_c$ | $b_c$ | $b_b$ | $h_b$ | $G$ | $(Av/s)_J$ | $(Av/s)_B$ | CFRP (Yes /No) |
|---|---|---|---|---|---|---|---|---|
| C1-MaJ-X1B-0 | 0.4 m | 0.4 m | 0.4 m | 0.36 m | 1.37 | 4.5 | 1.74 | No |
| C1-MaJ-X0B-0 | 0.4 m | 0.4 m | 0.4 m | 0.36 m | 1.37 | 4.5 | 0.78 | No |
| C2-MaJ-X1B-0 | 0.4 m | 0.4 m | 0.4 m | 0.29 m | 2.62 | 4.5 | 1.74 | No |
| C2-MaJ-X0B-0 | 0.4 m | 0.4 m | 0.4 m | 0.29 m | 2.62 | 4.5 | 0.78 | No |
| C1-MiJ-X1B-0 | 0.4 m | 0.4 m | 0.4 m | 0.36 m | 1.37 | 0.5 | 1.74 | No |
| C1-MiJ-X0B-0 | 0.4 m | 0.4 m | 0.4 m | 0.36 m | 1.37 | 0.5 | 0.78 | No |
| C2-MiJ-X1B-0 | 0.4 m | 0.4 m | 0.4 m | 0.29 m | 2.62 | 0.5 | 1.74 | No |
| C2-MiJ-X0B-0 | 0.4 m | 0.4 m | 0.4 m | 0.29 m | 2.62 | 0.5 | 0.78 | No |

force ($0.85P_p$), deflection at yield force ($\Delta_y$), deflection at peak force ($\Delta_p$) and deflection corresponding to $0.85P_p$ ($\Delta_u$). Moreover, Table 8 shows that as the relative gross inertia decreases, the ultimate capacity increases and the ductility decreases. This is logical because decreasing G means a larger beam. This trend also exists in the case of using CFRP

## 4. Data fitting

MATLAB software is used to develop ductility equations using the multivariable fitting tool. The procedure used in the fitting is as follows: First, a data set containing results from the parametric study is used to fit the equations by minimizing the norm of error between the equation and the data points. Then the equations are simplified. After that, another independent set of F.E. simulation data is used to verify the fitted equations. The primary variables for the equation are selected to be the relative gross inertia($G$), shear reinforcement in the beam $(Av/s)_B$and shear reinforcement in the joint $(Av/s)_J$ with and without CFRP for a constant longitudinal reinforcement ratio for the beam and column.

### 4.1. Ductility equation for exterior R.C beam-column joint without CFRP

Generally, two equations of ductility are proposed due to the large variations in the ductility of the joints due to the variable effect of shear failure in the beam and other types of failure. The first equation is for joints with brittle failure while the other for ductile failure. However, to predict which failure mode will happen; ACI 318 [36] code equations for shear and bending capacities are used and compared as shown in Eqs. (3)–(8).

$$P_{av} = V_{acb} + V_{asb} \tag{3}$$

$$V_{acb} = \frac{1}{6}\sqrt{f_c`}\, b_w d \quad \text{(ACI-318 [36])} \tag{4}$$

$$V_{asb} = \frac{Av}{s} f_y d \ \text{(ACI-318 [36])} \tag{5}$$

$$M_{af} = b_w d^2 \rho f_y \left(1 - \frac{\rho f_y}{1.7 f_c`}\right) \text{(ACI-318 [36])} \tag{6}$$

$$P_{af} = \frac{M_{af}}{L_t} \tag{7}$$

$$\gamma = \frac{P_{av}}{P_{af}} \tag{8}$$

where

$P_{av}$: Approximated shear capacity of the beam (N)
$V_{acb}$: Approximated shear capacity of the concrete beam (N)
$V_{asb}$: Approximate shear capacity of stirrups in the beam (N).
$f_c`$: Compressive strength of concrete (MPa).
$b_w$: Width of cross section (mm).
$d$: Effective depth of cross section of the beam (mm).
$Av$: Area of stirrups that resists shear force in the beam ($mm^2$).
$s$: Spacing between stirrups in the beam (mm).
$f_y$: yield stress of stirrups (MPa).
$M_{af}$: Approximated moment capacity of the beam (N.mm).
$\rho$: Longitudinal reinforcement ratio.
$P_{af}$: Approximated flexural load capacity of the beam (N)
$L_t$: Total length of the beam (mm) (model length which presents one-fourth of the total beam length) and is taken to be 900 mm in this research.
$\gamma$: Factor for predicting the type of failure. (For brittle failure, $\gamma \leq 1$ while $\gamma > 1$ for ductile failure).

Multivariable surface fitting was done in MATLAB as shown in Figs. 17 and 18 for brittle and ductile failures, respectively. As a result of these fittings, the surface equations are obtained as a function of the mentioned three variables. The relation between ductility and both variables ($G$) and $(Av/s)_B$ is directly proportional. However, the relation is inversely proportional between ductility and $(Av/s)_J$ as shown in Eqs. (9) and (10). According to the study, the proposed equations are based on ductility values between 1.3 and 7.5

The final equations from these surfaces fitting are:

$$D_0 = -0.50 + 2.40\sqrt{G} + 0.70\frac{\left(\frac{Av}{s}\right)_B}{\left(\frac{Av}{s}\right)_J}, for \gamma \leq 1 \tag{9}$$

$$D_0 = 1.0 + 3.0\sqrt{G} + 0.010\frac{\left(\frac{Av}{s}\right)_B}{\left(\frac{Av}{s}\right)_J}, for \gamma > 1 \tag{10}$$

where

$D_0$: Ductility of exterior reinforced beam- column joint without CFRP
$G$: Relative gross inertia of column to beam ($I_C/I_B$)
$s$: Spacing between stirrups.
$Av$: Area of stirrups that resists shear force.

An independent set of data points is generated by ABAQUS to check the validity of the Eqs. (7) and (8). Ductility of eight independent models with properties as shown in Table 9 is calculated numerically and compared with the results from Eqs. (9) and (10). The values of variables($G$), and $(Av/s)_B$ are selected to be within the range of the parameters used earlier in this paper. Moreover, Fig. 19 shows the Load deflection curves of these models. In addition, Table 10 shows the summary of the results of these models, while Table 11 shows a comparison between ABAQUS ductility and ductility from Eqs. (9) and (10) for all models without CFRP. It can be seen that the maximum percent of difference between ductility from ABAQUS and ductility from the equations is approximately15%.

### 4.2. Ductility equation for exterior reinforced beam-column joint with CFRP

Multivariable surface fitting was done also in MATLAB for beam-column joints with CFRP as shown in Fig. 20. Eq. (11) proposed the ductility equation using the same variables of the study. The proposed

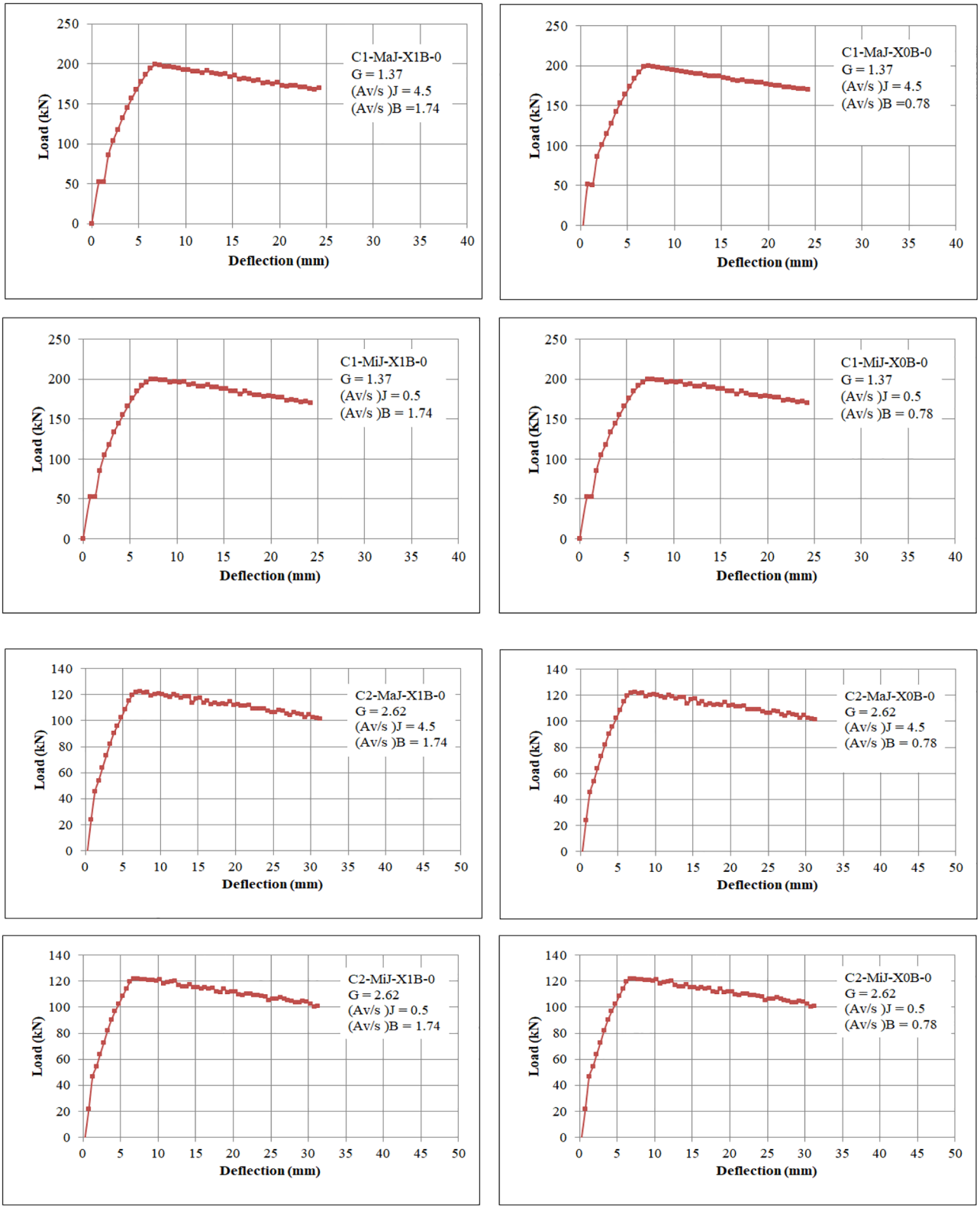


**Fig. 19.** Load deflection curves for independent models without CFRP.

**Table 10**
Results of independent models without CFRP.

| Model | $P_y$ (kN) | $P_P$ (kN) | $0.85P_p$ (kN) | $\Delta_y$ (mm) | $\Delta_p$ (mm) | $\Delta_u$ (mm) | Ductility ($\frac{\Delta_u}{\Delta_y}$) |
|---|---|---|---|---|---|---|---|
| C1-MaJ-X1B-0 | 177 | 199 | 169.15 | 5.1 | 6.8 | 24.26 | 4.76 |
| C1-MaJ-X0B-0 | 177 | 199 | 169.15 | 5.1 | 6.8 | 24.25 | 4.75 |
| C2-MaJ-X1B-0 | 108 | 122 | 103.7 | 5.1 | 6.8 | 31 | 6.08 |
| C2-MaJ-X0B-0 | 108 | 121 | 102.85 | 5.1 | 6.8 | 30 | 5.88 |
| C1-MiJ-X1B-0 | 177 | 199 | 169.15 | 5.1 | 6.8 | 24.26 | 4.76 |
| C1-MiJ-X0B-0 | 177 | 199 | 169.15 | 5.1 | 6.8 | 24.25 | 4.75 |
| C2-MiJ-X1B-0 | 108 | 122 | 103.7 | 5.1 | 6.8 | 31 | 6.08 |
| C2-MiJ-X0B-0 | 108 | 121 | 102.85 | 5.1 | 6.8 | 30 | 5.88 |

**Table 11**
Comparing ABAQUS results and equation results for joints without CFRP.

| Model | Ductility (ABAQUS) | Ductility (Eqs. (7) and (8)) | Relative difference = 100%. $\frac{D_{ABAQUS} - D_{Equation}}{D_{ABAQUS}}$ |
|---|---|---|---|
| G1-MaJ-MiB-0 | 1.24 | 1.3 | −4.84 |
| G1-MaJ-B1B-0 | 1.64 | 1.4 | 14.63 |
| G1-MaJ-B2B-0 | 3.23 | 3.15 | 2.47 |
| G1-MaJ-MaB-0 | 3.23 | 3.15 | 2.47 |
| G2-MaJ-MiB-0 | 1.76 | 1.98 | −12.5 |
| G2-MaJ-B1B-0 | 4.45 | 4 | 10.11 |
| G2-MaJ-B2B-0 | 4.6 | 4 | 13.04 |
| G2-MaJ-MaB-0 | 4.6 | 4.01 | 12.83 |
| G3-MaJ-MiB-0 | 7.27 | 7.45 | −2.48 |
| G3-MaJ-B1B-0 | 7.31 | 7.46 | −2.05 |
| G3-MaJ-B2B-0 | 7.37 | 7.46 | −1.22 |
| G3-MaJ-MaB-0 | 7.4 | 7.46 | −0.81 |
| G1-MiJ-MiB-0 | 1.95 | 1.92 | 1.54 |
| G1-MiJ-B1B-0 | 2.73 | 2.8 | −2.56 |
| G1-MiJ-B2B-0 | 2.8 | 3.2 | −14.3 |
| G1-MiJ-MaB-0 | 2.8 | 3.23 | −14.98 |
| G2-MiJ-MiB-0 | 2.9 | 2.5 | 13.8 |
| G2-MiJ-B1B-0 | 4 | 4.02 | −0.5 |
| G2-MiJ-B2B-0 | 4 | 4.06 | −1.5 |
| G2-MiJ-MaB-0 | 4 | 4.09 | −2.25 |
| G3-MiJ-MiB-0 | 7.27 | 7.46 | −2.61 |
| G3-MiJ-B1B-0 | 7.27 | 7.48 | −2.9 |
| G3-MiJ-B2B-0 | 7.31 | 7.52 | −2.87 |
| G3-MiJ-MaB-0 | 7.31 | 7.54 | −3.15 |
| C1-MaJ-X1B-R | 4.76 | 4.52 | 5.04 |
| C1-MaJ-X0B-R | 4.75 | 4.51 | 5.05 |
| C2-MaJ-X1B-R | 6.08 | 5.86 | 3.62 |
| C2-MaJ-X0B-R | 5.88 | 5.86 | 0.34 |
| C1-MiJ-X1B-R | 4.76 | 4.55 | 4.4 |
| C1-MiJ-X0B-R | 4.75 | 4.53 | 4.63 |
| C2-MiJ-X1B-R | 6.08 | 5.89 | 3.13 |
| C2-MiJ-X0B-R | 5.88 | 5.87 | 0.2 |

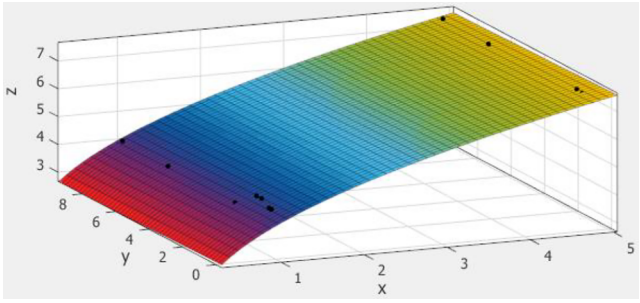


**Fig. 20.** Surface ductility fitting for joints with CFRP.

equations of the ductility of the joints strengthened with CFRP is bounded by ductility values between 3 and 7.5 as shown in Table 8.

The final equation from this fitting is:

$$D_{CFRP} = 1.0 + 3.0\sqrt{G} + 0.010\frac{\left(\frac{Av}{s}\right)_B}{\left(\frac{Av}{s}\right)_J} \quad (11)$$

where

$D_{CFRP}$: Ductility of exterior reinforced beam- column joint with CFRP

An independent set of data points is generated by ABAQUS to check the validity of Eq. (9). Ductility of eight independent models with properties as shown in Table 11 but with adding CFRP sheets is calculated numerically and compared with the results from Eq. (11). Moreover, Fig. 21 shows the load deflection curves of these models. In addition, Table 12 shows the summary of the results of these models, while Table 13 shows the comparisons between ABAQUS ductility and the ductility from Eq. (11) for all models with CFRP. It can be seen that the maximum percent of the difference between the ductility from ABAQUS and the ductility from the equation is approximately 15%.

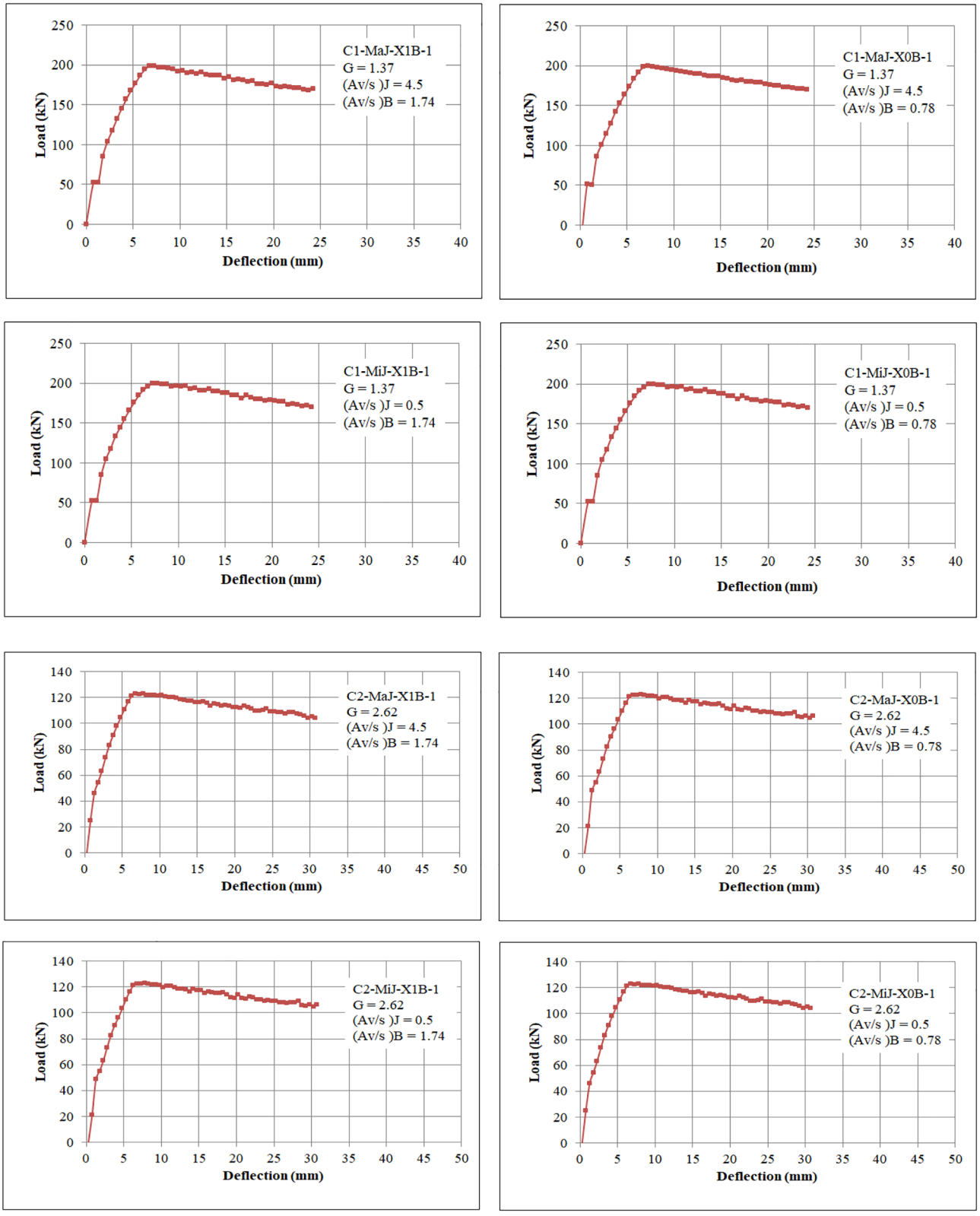


**Fig. 21.** Load deflection curves for independent models with CFRP.

### *4.3. Limitations of the proposed equations*

As shown before, the maximum percent of error between the numerical results and the proposed equations is less than 15% for all cases. However, these equations can be used in many cases to predict the behavior of the structure in a simplified nonlinear analysis process.

It must be noted that the previously mentioned equations (Eqs. (9)–(11)) have limitations that must be considered. These equations are valid under the following limitations:

1- These equations can be used for exterior R.C beam-column joints only.

**Table 12**
Results of independent models with CFRP.

| Model | $P_y$ (kN) | $P_P$ (kN) | $0.85P_P$ (kN) | $\Delta_y$ (mm) | $\Delta_p$ (mm) | $\Delta_u$ (mm) | Ductility ($\frac{\Delta_u}{\Delta_y}$) |
|---|---|---|---|---|---|---|---|
| C1-MaJ-X1B-1 | 180 | 202.3 | 171.955 | 5.1 | 6.8 | 25.2 | 4.94 |
| C1-MaJ-X0B-1 | 180 | 202 | 171.7 | 5.1 | 6.8 | 25 | 4.9 |
| C2-MaJ-X1B-1 | 106 | 122.7 | 104.295 | 5.1 | 6.8 | 31 | 6.08 |
| C2-MaJ-X0B-1 | 106 | 122.6 | 104.21 | 5.1 | 6.8 | 30 | 5.9 |
| C1-MiJ-X1B-1 | 180 | 202.3 | 171.955 | 5.1 | 6.8 | 25.2 | 4.94 |
| C1-MiJ-X0B-1 | 180 | 202.3 | 171.955 | 5.1 | 6.8 | 25 | 4.92 |
| C2-MiJ-X1B-1 | 106 | 122.7 | 104.295 | 5.1 | 6.8 | 31 | 6.08 |
| C2-MiJ-X0B-1 | 106 | 122.6 | 104.21 | 5.1 | 6.8 | 30 | 5.88 |

**Table 13**
Comparing ABAQUS results and equation results for joints with CFRP.

| Model | Ductility (ABAQUS) | Ductility (equation 5.9) | Relative difference = 100%. $\frac{D_{ABAQUS} - D_{Equation}}{D_{ABAQUS}}$ |
|---|---|---|---|
| G1-MaJ-MiB-1 | 3.03 | 3.15 | −4 |
| G1-MaJ-B1B-1 | 3.03 | 3.15 | −4 |
| G1-MaJ-B2B-1 | 3.1 | 3.15 | −1.61 |
| G1-MaJ-MaB-1 | 3.1 | 3.15 | −1.61 |
| G2-MaJ-MiB-1 | 4.45 | 4 | 10.11 |
| G2-MaJ-B1B-1 | 4.45 | 4 | 10.11 |
| G2-MaJ-B2B-1 | 4.65 | 4 | 14 |
| G2-MaJ-MaB-1 | 4.65 | 4.01 | 13.76 |
| G3-MaJ-MiB-1 | 7.31 | 7.45 | −1.92 |
| G3-MaJ-B1B-1 | 7.31 | 7.46 | −2.05 |
| G3-MaJ-B2B-1 | 7.38 | 7.46 | −1.08 |
| G3-MaJ-MaB-1 | 7.44 | 7.46 | −0.27 |
| G1-MiJ-MiB-1 | 2.72 | 3.15 | −14.97 |
| G1-MiJ-B1B-1 | 2.72 | 3.15 | −14.97 |
| G1-MiJ-B2B-1 | 2.79 | 3.2 | −14.69 |
| G1-MiJ-MaB-1 | 2.79 | 3.2 | −14.69 |
| G2-MiJ-MiB-1 | 3.94 | 4.01 | −1.78 |
| G2-MiJ-B1B-1 | 4 | 4.02 | −0.5 |
| G2-MiJ-B2B-1 | 4.04 | 4.06 | −0.5 |
| G2-MiJ-MaB-1 | 4.08 | 4.09 | −0.25 |
| G3-MiJ-MiB-1 | 7.31 | 7.46 | −2.05 |
| G3-MiJ-B1B-1 | 7.331 | 7.48 | −2.03 |
| G3-MiJ-B2B-1 | 7.38 | 7.52 | −1.89 |
| G3-MiJ-MaB-1 | 7.44 | 7.54 | −1.34 |
| C1-MaJ-X1B-1 | 4.94 | 4.52 | 8.5 |
| C1-MaJ-X0B-1 | 4.9 | 4.51 | 7.96 |
| C2-MaJ-X1B-1 | 6.08 | 5.86 | 3.62 |
| C2-MaJ-X0B-1 | 5.9 | 5.86 | 0.68 |
| C1-MiJ-X1B-1 | 4.94 | 4.55 | 7.89 |
| C1-MiJ-X0B-1 | 4.92 | 4.53 | 7.93 |
| C2-MiJ-X1B-1 | 6.08 | 5.89 | 3.13 |
| C2-MiJ-X0B-1 | 5.88 | 5.87 | 0.17 |

2- Ratio between moment and shear loads on the joint approximately equals 1.
3- Relative gross inertia ($G$)between 0.512 until to 4.63 (these values are common and realistic).
4- Flexural steel ratio for the beam and the column is close to 1% (this value is common and realistic).
5- Axial load/ axial capacity of the column is close to 0.3.
6- No axial force in the beam.

## 5. Conclusions

In this study, numerical F.E results of exterior CFRP-strengthened beam column R.C joints were used to predict the rotational ductility of such joints considering realistic constant axial load ratio. Load-deflection curves of 48 beam-column joints were analyzed and used to define ductility and failure type of the joints which were categorized using different parameters. Based on the findings of this work, the following conclusions are drawn:

- The developed F.E. model produced realistic and accurate results, and captured the nonlinear complex behavior of the joint. The results clearly show that using CFRP wraps around beams converts the brittle failure to ductile failure. However, there is a minor effect of CFRP as the confinement is majorly obtained due to the beam stirrups or when failure happens inside the joint. On the other hand, the effect of CFRP wrapping is significant for cases that are dominated by only shear failure of the beam.
- Material and geometrical nonlinearities, and proper contact model are used to reflect reality of full scale beam column joint models. Relative gross column-to-beam moment of inertia, shear reinforcement of the beam and joints are the main focus of the study considering the effect of each parameter on the ductility of joints with or even without CFRP.
- This study defines three main types of failure based on ductility values, flexural ductile beam failure, brittle shear beam and joint failure, in addition to a moderate case of ductility that shows joint failure. Ductility is defined as the ratio of the ultimate deflection to yielding deflection
- Simplified equations that predict the rotational ductility of CFRP-strengthened R.C joints are proposed through statistical regression

of numerical results generated by high-fidelity finite element simulations in ABAQUS. Proposed equations are able to calculate the ductility of R.C exterior joints with percent of error less than 15% under certain limitations.

- Simplified equations are proposed for CFRP strengthened and non-strengthened beam column joints separately. The equations consider the effect of relative gross column-to-beam moment of inertia, shear reinforcement of the beam in addition to shear reinforcement of the joint.
- Effectiveness of using CFRP to increase the beam-column joint ductility is a function of the failure type (i.e. ductile beam failure, brittle beam failure and joint failure). The CFRP is found to be most efficient in the case of the brittle beam failure as CFRP wraps are applied to the beams which suffered this type of failure.

## Declaration of Competing Interest

The authors declare that they have no known competing financial interests or personal relationships that could have appeared to influence the work reported in this paper.

## References


[1] Kaliluthin AK, Kothandaraman S, Ahamed TS. A review on behavior of reinforced concrete beam-column joint. Int J Innov Res Sci, Eng Technol 2014;3(4):11299–312.
[2] Uma SR, Prasad AM. Seismic behavior of beam column joints in reinforced concrete moment resisting frames. Chennai: Department of Civil Engineering, Indian Institute of technology Madras; 1996.
[3] ACI-ASCE. Recommendations for Design of Beam-Column Joints in Monolithic Reinforced Concrete Structures. Committee report 352R-85. American Concrete Institute, ACI Journal 1985; 1(3): 266-284.
[4] Ghobarah A, Said A. Shear strengthening of beam-column joints. Eng Struct 2002;24(7):881–8.
[5] Attari N, Amziane S, Chemrouk M. Flexural strengthening of concrete beams using CFRP, GFRP and hybrid FRP sheets. Constr Build Mater 2012;37:746–57.
[6] Ghobarah A, Said A. Seismic rehabilitation of beam-column joints using FRP laminates. J Earthquake Eng 2001;5(01):113–29.
[7] El-Amoury AT. Seismic Rehabilitation of Concrete Frame Beam-Column Joints (PhD. thesis). Ontario, Canada: McMaster University; 2004.
[8] Mahmoud MH, Afefy HM, Kassem NM, Fawzy TM. Strengthening of defected beam–column joints using CFRP. J Adv Res 2014;5(1):67–77.
[9] Samaaneh MA, Sharif AM, Baluch MH, Azad AK. Numerical investigation of continuous composite girders strengthened with CFRP. Steel Compos Struct 2016;21(6):1307–25.
[10] Halahla A, Rahman M, Algadhib A, Alosta M, Baluch M. Experimental investigations and FE simulation of exterior BCJs retrofitted with CFRP fabric. Earthquakes Struct 2019;17(4):337–54.
[11] Eslami A, Ronagh HR. Experimental investigation of an appropriate anchorage system for flange-bonded carbon fiber–reinforced polymers in retrofitted RC beam–column joints. J Compos Constr 2013;18(4):04013056.
[12] Esmaeeli E, Barros JA, Sena-Cruz J, Fasan L, Prizzi FR, Melo J, et al. Retrofitting of interior RC beam–column joints using CFRP strengthened SHCC: cast-in-place solution. Compos Struct 2015;122:456–67.
[13] Mostofinejad D, Akhlaghi A. Experimental investigation of the efficacy of EBROG method in seismic rehabilitation of deficient reinforced concrete beam–column joints using CFRP sheets. J Compos Constr 2016;21(4):04016116.
[14] Mostofinejad D, Hajrasouliha M. Shear retrofitting of corner 3D-reinforced concrete beam-column joints using externally bonded CFRP reinforcement on grooves. J Compos Constr 2018;22(5):04018037.
[15] Ilia E, Mostofinejad D. Seismic retrofit of reinforced concrete strong beam–weak column joints using EBROG method combined with CFRP anchorage system. Eng Struct 2019;194:300–19.
[16] Mostofinejad D, Hajrasouliha M. 3D beam–column corner joints retrofitted with X-shaped FRP sheets attached via the EBROG technique. Eng Struct 2019;183:987–98.
[17] Mostofinejad D, Akhlaghi A. Flexural strengthening of reinforced concrete beam-column joints using innovative anchorage system. ACI Struct J 2017;114(6):1603–14.
[18] Mostofinejad D, Akhlaghi A, Eslami A. Estimating the seismic performance of CFRP-retrofitted RC Beam-column connections using fiber-section analysis. J Earthquake Eng 2018;22(6):1092–110.
[19] Jing LI, Pam HJ, Francis TK. New details of HSC beam-column joints for regions of low to moderate seismicity. In: 13th World Conference on Earthquake Engineering, Vancouver, Canada; 2004.
[20] Tahnat YB, Dwaikat MM, Samaaneh MA. Effect of using CFRP wraps on the strength and ductility behaviors of exterior reinforced concrete joint. Compos Struct 2018;201:721–39.
[21] Hajrasouliha M, Mostofinejad D. Effect of lateral beam on the seismic behavior of corner RC beam–column joints under cyclic reversal loading. Eur J Environ Civil Eng 2019:1–5.
[22] Alavi-Dehkordi S, Mostofinejad D, Alaee P. Effects of high-strength reinforcing bars and concrete on seismic behavior of RC beam-column joints. Eng Struct 2019;183:702–19.
[23] Clyde C, Pantelides CP, Reaveley LD. Performance-based evaluation of exterior reinforced concrete building joints for seismic excitation. Berkeley: Pacific Earthquake Engineering Research Center, College of Engineering, University of California; 2000.
[24] Chaudhari SV, Mukane KA, Chakrabarti MA. Comparative study on exterior RCC beam column joint subjected to monotonic loading. Int J Comput Appl 2014;102(3).
[25] Alfarah B, López-Almansa F, Oller S. New methodology for calculating damage variables evolution in Plastic Damage Model for RC structures. Eng Struct 2017;132:70–86.
[26] Najafgholipour MA, Dehghan SM, Dooshabi A, Niroomandi A. Finite element analysis of reinforced concrete beam-column connections with governing joint shear failure mode. Latin Am J Solids Struct 2017;14(7):1200–25.
[27] Ghobarah A, Biddah A, Mahgoub M. Rehabilitation of reinforced concrete columns using corrugated steel jacketing. J Earthquake Eng 1997;1(04):651–73.
[28] Sadone R, Quiertant M, Mercier J, Ferrier E. Experimental study on RC columns retrofitted by FRP and subjected to seismic loading. 6th International Conference on FRP Composites in Civil Engineering, Ontario, Canada. 2012.
[29] Al-Salloum YA, Al-Sayed SH, Al-Musallam TH, Siddiqui NA. Seismic performance of shear deficient exterior RC beam-column joints repaired using CFRP composites. Saudi Engineering Conference, Dhahran, Saudi Arabia. 2002.
[30] Wahalathantri BL, Thambiratnam DP, Chan THT, Fawzia S. Material model for flexural crack simulation in reinforced concrete elements using ABAQUS. First International Conference on Engineering, Designing and Developing the Built Environment for Sustainable Wellbeing. 2011. p. 260–4.
[31] ABAQUS. ABAQUS Analysis User's Manual Version 6.13, Assault Systems; 2013.
[32] Saenz LP. Equation for the stress-strain curve of concrete. ACI J 1964;61(9):1229–35.
[33] Asran G, EL-Esnawi H, Fayed S. Numerical investigation of RC exterior beam colum connections under monotonic loads. J Mech Civil Eng 2016;13(1):60–7.
[34] Halahla AM, Tahnat YB, Almasri AH, Voyiadjis GZ. The effect of shape memory alloys on the ductility of exterior reinforced concrete beam-column joints using the damage plasticity model. Eng Struct 2019;200:109676.
[35] Sharif AM, Samaaneh MA, Azad AK, Baluch MH. Use of CFRP to maintain composite action for continuous steel–concrete composite girders. J Compos Constr 2015;20(4).
[36] ACI. Building Code Requirements for Structural Concrete. Committee report 318-14, American Concrete Institute, Detroit, Michigan; 2014.
[37] Mallick PK. Fiber-reinforced composites. New York: Marcel Dekker; 1993.
[38] Neubauer U, Rostasy FS. Bond failure of concrete fiber reinforced polymer plates at inclined cracks—experiments and fracture mechanics model. Proc., 4th Int. Symp. on Fiber-Reinforced Polymer Reinforcement for Reinforced Concrete Structures, SP-188. Farmington Hills, Mich: American Concrete Institute; 1999. p. 369–82.
[39] Obaidat YT, Heyden S, Dahlblom O. Bond action between FRP and concrete–a new model. Structural Retrofitting of Concrete Beams Using FRP; 2011.
[40] Park RL, Park R, Paulay T. Reinforced concrete structures. New York: John Wiley & Sons; 1975.